Estimating Corn Biomass from RGB Images Acquired with an Unmanned Aerial Vehicle

K. Khun[1], P. Vigneault[2], E. Fallon[2], N. Tremblay[2], C. Codjia[3], F. Cavayas[1]

1. Department of Geography, Université de Montréal, Montreal, Quebec, Canada

2. St-Jean-sur-Richelieu Research and Development Center, Agriculture and Agri-Food Canada, St-Jean-sur-Richelieu, Quebec, Canada

3. Department of Geography, Université du Québec à Montréal, Montreal, Quebec, Canada

A paper from the Proceedings of the
14th International Conference on Precision Agriculture
June 24 – June 27, 2018
Montreal, Quebec, Canada

Abstract.

Above-ground biomass, along with chlorophyll content and leaf area index (LAI), is a key biophysical parameter for crop monitoring. Being able to estimate biomass variations within a field is critical to the deployment of precision farming approaches such as variable nitrogen applications.

With unprecedented flexibility, Unmanned Aerial Vehicles (UAVs) allow image acquisition at very high spatial resolution and short revisit time. Accordingly, there has been an increasing interest in those platforms for crop monitoring and precision agriculture. Typically, classic remote sensing techniques tend to rely on a vegetation index – such as the popular Normalized Difference Vegetation Index (NDVI) – as a proxy for plant biophysical parameters. However, when applied to UAV imagery, those approaches do not fully exploit the greater details provided by high resolution.

The purpose of this research is to develop a procedure for assessing above-ground biomass based on the analysis of very high resolution RGB imagery acquired with a UAV platform. A small consumer-grade UAV (the DJI Phantom 3 Professional) with a built-in RGB camera was flown over an experimental corn (Zea mays L.) field. A series of images were acquired in summer 2017 at very low altitudes, resulting in milli-resolution imagery (images with less than 1 cm per pixel). Two modes of image acquisition were performed: in a grid pattern at an altitude of 10m AGL (above ground level) for generating orthomosaics, and in a stationary mode at a height of 2.9m AGL. For stability reasons, the latter mode was simulated by a low-altitude platform hung on a zip-line.

Image acquisitions were repeated in time during the early stages of corn growth, covering phenological stages from V2 to V8. Oblique imagery was also acquired in order to evaluate the effect of viewing angle. Field measurement campaigns were carried out in order to provide quantitative measurements of some biophysical parameters, including plant fresh biomass,

plant dry biomass, plant height, leaf fresh biomass and leaf dry biomass. The method proposed in this study is based on computer vision, which allowed extracting leaf projected area from the images for estimating biomass and detecting differences in corn growth. Using UAV-derived imagery to extract information on biomass proves to be a cost-effective means for monitoring crop biomass spatially and temporally.

Keywords.
UAV, DJI Phantom, RGB imagery, biomass, corn, leaf projected area, image processing, low altitude remote sensing, precision agriculture.

Introduction

Monitoring crop vigor is the more crucial at early season as many decisions related to crop management are made when the plant is still at early growth stage. Assessing crop growth status is often done through proximal sensors installed onboard a tractor. Usually, a vegetation index (VI) such as the NDVI - Normalized Difference Vegetation Index - is used to estimate crop vigor (Bouroubi et al. 2013). Above-ground biomass is an effective proxy of measuring crop vigor and therefore is a good biophysical parameter for crop management (Yu et al. 2013). It allows a better assessment of spatial variability in the field and a finer management of nitrogen applications. Even though VIs have been found to correlate with some biophysical characteristics such as leaf area index (LAI) or biomass, their use in the context of high spatial resolution images acquired by UAVs becomes a challenge (Hunt et al. 2013).

Most vegetation indices use two specific spectral bands (Xue and Su 2017): the red band (around 650nm) and the near infrared band (around 800nm). However, images taken with a multispectral camera have to be radiometrically normalized, because the digital values are dependent on lighting conditions and sensor opto-geometric parameters. Therefore, radiometric corrections are necessary to reduce the effects of vignetting (Lelong et al. 2008), bidirectional reflectance distribution function or BRDF (Lelong et al. 2008) or atmospheric noise (Berni et al. 2009). Furthermore, a typical multispectral camera is in fact an aggregation of separate sensors, mounted close to each other, each acquiring information at a specified bandwidth. The resulting band images need to be aligned (Rabatel and Labbé 2016). At very high spatial resolution, this band-to-band registration needs to be perfectly done, with sub-pixel accuracy.

The objective of this paper is to explore another approach of assessing corn biomass at early growth stages, using only a consumer-grade RGB camera aboard a UAV. Leaf projected area was extracted from mosaics generated from UAV imagery and was compared with biomass measured in situ. Finally, images taken at zero zenith angle are compared with oblique imagery to examine whether a significant improvement can be achieved when photos are taken with an angle relative to the vertical.

Materials and methods

Field site

The experiment was conducted in July and August 2017, at the experimental farm of L'Acadie, St-Jean-sur-Richelieu Research and Development Center, Agriculture and Agri-Food Canada, St-Jean-sur-Richelieu, Quebec, Canada (45°17'40.092" N, 73°20'45.0168" W). A 0.5ha corn field (100m x 50m) was chosen for the experiment. Field corn (Zea mays L.) was planted in strips of four rows, each row being 75cm apart and each strip being 3m apart. A total of 15 strips were used, with different sowing dates so that a variety of stages (between V2 and V8) were met during each field campaign.

Biomass measurement

During the experiment, a weekly ground-truthing campaign was carried out to collect biomass and other biophysical parameters of corn. Each sampling point was randomly chosen and consisted of an area covering two rows of ten consecutive plants each. Following the image acquisition, each plant was sampled individually: its fresh biomass and dry biomass were measured and used as ground truth to correlate with the information extracted from low altitude remote sensing images.

Image acquisition platforms and image preprocessing

Two types of platforms were used for this experiment. First, a commercial UAV, the Phantom 3

Professional (DJI, Shenzhen, China), with a built-in camera (hereinafter *camera P*), was used to acquire images at very high spatial resolution, in a grid pattern mode. The UAV was flown at an altitude of 10m above ground level, which resulted in a ground sampling distance (GSD) of 4.4mm per pixel. In order to increase image stitching success, flight paths were planned with a minimum overlap of 70% (side-lap and forward-lap). For each acquisition date, the raw images were imported into Pix4Dmapper Pro software (Pix4D, Lausanne, Switzerland) and a georectified orthomosaic was generated using ground control points (GCPs) located in the fields and positioned with an RTK-based GPS receiver (SXBlue III-L, Geneq Inc., Montreal, Quebec, Canada).

A stationary mode was also tested where each sampled row would be photographed with the UAV hovering above. However, for stability reasons and ease of manipulation, a custom-built platform was devised with a consumer-grade RGB camera (Canon SX230 HS, Canon Inc., Tokyo, Japan [hereinafter *camera C*]) mounted on a low-altitude platform hung on a zip-line at a height of 2.90m (Fig. 1). The camera was remotely operated and could take oblique pictures with viewing angles of 0° (nadir), 30° and 45° relative to the vertical. The geometric distortions due the camera lens were roughly corrected by the camera internal software and no further preprocessing was done.

Fig 1. RGB camera mounted on a zip-line (camera C).

The technical characteristics of both cameras are shown below (Table 1). Both cameras had the same sensor type, but the focal length of camera P was shorter (3.6mm vs 5mm), which means that an image from camera C would exhibit a smaller GSD – i.e. a higher spatial resolution – than that of camera P when taken from the same distance. The GSD was calculated at the center of the image, and for oblique imagery, it varied with the viewing angle: the platform height being constant, the distance between the camera and the target had to be adjusted.

Table 1. Technical specifications of cameras used for image acquisition

	Camera P (UAV built-in camera)	Camera C (Canon SX230 HS)
Sensor	1/2.3" CMOS	1/2.3" CMOS
Sensor width	6.3mm	6.16mm
Sensor height	4.73mm	4.62mm
Image size	4000 x 3000	4000 x 3000
Focal length	3.6mm	5mm
Pixel pitch	1.58µm	1.54µm
Platform altitude	10m AGL	2.9m AGL
Ground sampling distance (GSD)	4.4mm (orthomosaic)	0.89mm (viewing angle=0°) 1.03mm (viewing angle=30°) 1.26mm (viewing angle=45°)

Image processing

In order to compare both platforms and their results with the ground truth, sampling areas needed to be manually delimited in the images. That task was done with the help of a custom-built graphic user interface (GUI), developed in the Python programming language (Python Software Foundation, https://www.python.org) using the Tk GUI toolkit. Then the images were segmented in order to discriminate vegetation from the background. Finally, the projected area of plants was calculated and correlated with in situ measurements of biomass.

Delimiting sampling areas

For camera P, orthomosaics generated from UAV imagery were first clipped into smaller images of approximately 800 x 800pixels (around 3.5m x 3.5m), each centered on a sampling area.

Within each image, the 2 sampled rows with their 20 plants were further identified and each row was delimited with a rectangle (Fig. 2a).

For camera C, each image was processed individually: the plants of interest were enclosed by a 1m long rectangle centered on the sampled row and only plants contained in that rectangle were used as ground truth (Fig. 2b). Within nadir images (with a viewing angle of 0°), the rectangle width corresponded to the inter-row spacing, i.e. 0.75m (Fig. 2b). For oblique images (with a viewing angle of 30° and 45°), the rectangle was wider to encompass the entire height of corn plants (Fig. 3a and 3b).

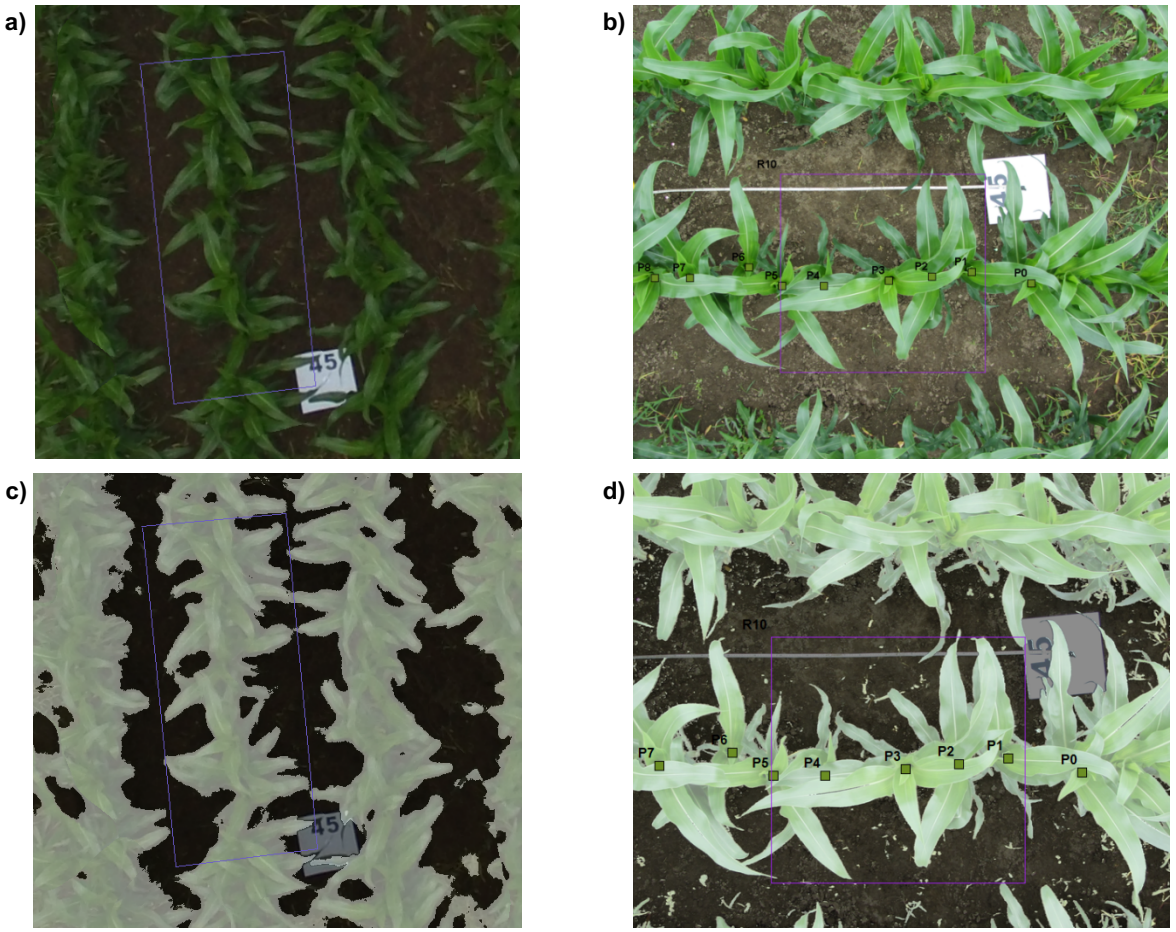

Fig 2. Screenshots excerpted from the custom-built GUI showing a sampling area in nadir imagery: (a) clipped orthomosaic from camera P and (b) RGB image from camera C, and their respective segmented images superimposed on the original photos (c and d). Ground control point (GCP) number 45 can be seen here, helping locate the sampling area. Numbers P0 to P9 identify each plant in the sampled row, enclosed within rectangle R10.

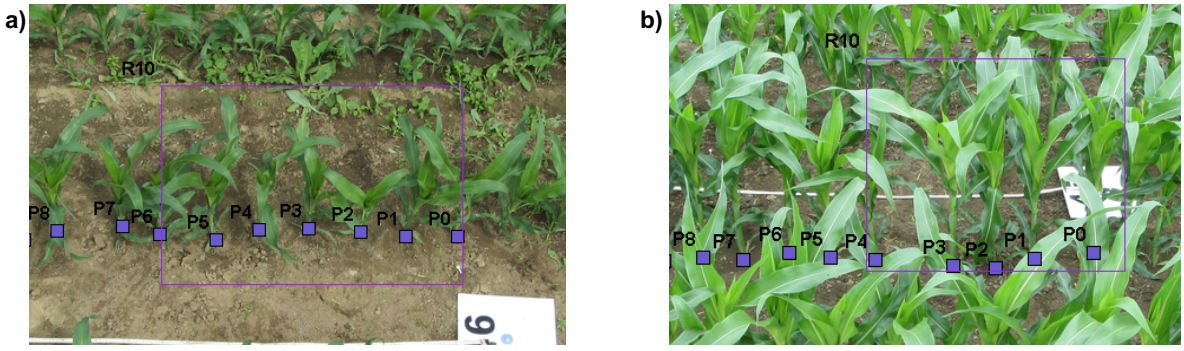

Fig 3. Oblique images of a sampling area photographed with camera C at viewing angles of (a) 30° and (b) 45° relative to the vertical. Numbers P0 to P9 identify each plant in the sampled row, enclosed within rectangle R10.

Image segmentation

The image segmentation was entirely carried out with a Python script using modules such as OpenCV and NumPy. From each RGB image, a color index (CI) was generated, allowing the image to be binarized by thresholding. Using a CI had the advantage of combining the information within the 3 bands (red, green and blue) into one synthetic band that accentuated a specific color, such as plant greenness. It helped then distinguish intuitively a class of interest, such as green plants, from the background (bare soil and residues mainly, and sometimes weeds, even though weeding was always performed before data acquisition). The CI that was chosen was the Excess Green minus Excess Red (ExG – ExR) index, proposed by Meyer and Neto (2008). It was proven to work especially well and was more accurate than other CIs.

Excess Green (ExG) was one of five CIs originally tested by Woebbecke et al. (1995) for distinguishing living material from bare soil and residues, while Excess Red (ExR) was proposed by Meyer et al. (1999), see equations (1) and (2) respectively.

Excess Green: $$\mathbf{ExG} = 2\boldsymbol{g} - \boldsymbol{r} - \boldsymbol{b} \quad (1)$$

Excess Red: $$\mathbf{ExR} = 1.4\boldsymbol{r} - \boldsymbol{g} \quad (2)$$

where $\boldsymbol{r}, \boldsymbol{g}, \boldsymbol{b}$ are the normalized RGB values defined as:

$\boldsymbol{r} = \frac{\boldsymbol{R}}{\boldsymbol{R+G+B}}$, $\boldsymbol{g} = \frac{\boldsymbol{G}}{\boldsymbol{R+G+B}}$, and $\boldsymbol{b} = \frac{\boldsymbol{B}}{\boldsymbol{R+G+B}}$

and ***R***, ***G***, and ***B*** are 2D matrices of pixel values in the red, green and blue channels respectively.

The ExG – ExR index is thus simply the difference between the two previous CIs:

$$\mathbf{ExG} - \mathbf{ExR} = 3\boldsymbol{g} - 2.4\boldsymbol{r} - \boldsymbol{b} \quad (3)$$

Unlike most CIs that require the calculation of a threshold value (using the Otsu's method, e.g.), which varies from one image to another, ExG – ExR has a constant threshold of zero: plant pixels have positive values whereas background pixels have negative values.

Leaf projected area

For each RGB image, the segmentation step generated a binary image where pixels corresponding to plants had a value of 1 and background pixels had a value of 0. By extracting all the pixels under the sampling rectangle and by summing their values, it was then possible to automatically count the number of plant pixels within the sampling zone. A leaf projected area (LA) value could then be calculated as:

$$\mathrm{LA} = N\rho^2 \quad (4)$$

where N = number of plant pixels, and ρ = ground sampling distance (GSD).

It should be noted that the counted pixels included both leaves and stems of the plants, especially when viewing from an oblique angle. Furthermore, the calculated area was considered projected because all pixels were given the same nominal GSD regardless of their actual distance to the camera: the 3D position of each pixel was unknown.

Finally, the LA values were normalized per unit length so they could be compared on the same scale:

$$\widehat{\mathrm{LA}} = \frac{N\rho^2}{\ell} \quad (5)$$

where ℓ = sampling zone length.

Results and Discussion

Comparison between acquisition platforms

There was a linear relationship between $\widehat{\mathrm{LA}}$ calculated from both platforms (Fig. 4), with a high determination coefficient (R^2 = 0.93). Although images acquired with camera P were expected to be less accurate because of a larger GSD (five times that of camera C, i.e. a lower spatial resolution for camera P), blurring due to UAV motion and pixel interpolating for orthomosaic generation, both cameras yielded almost the same results. As long as the spatial resolution is high enough, image segmentation will output consistent information. Rasmussen et al. (2013) also found that crop/soil segmentation at early growth stages in barley required ultrafine-resolution images (GSD < 5mm). In this experiment, the maximum GSD was 4.4mm for camera P and 1.26mm for camera C.

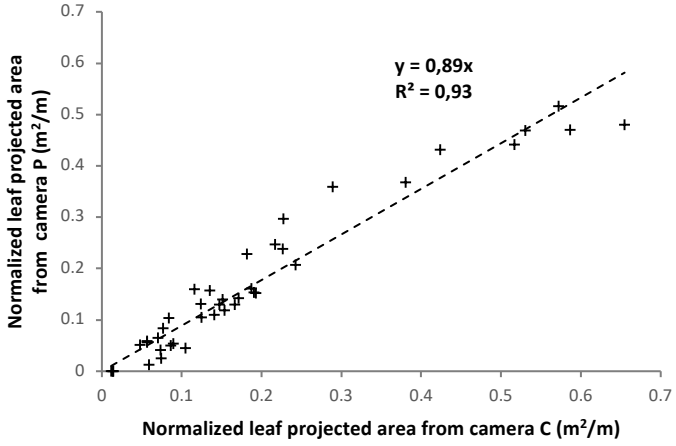

Fig 4. Relationship between normalized leaf projected areas $\widehat{\mathrm{LA}}_C$ from Canon camera and $\widehat{\mathrm{LA}}_P$ from UAV camera. Sample size N=42.

When comparing $\widehat{LA}$ values with ground truth data, Figure 5 shows that there was generally a good correlation between $\widehat{LA}$ and biomass (R^2 varying from 0.73 to 0.89). More precisely, for both cameras, R^2 was higher in the case of fresh biomass than dry biomass. Camera C gave a better correlation than camera P (R^2=0.89 vs R^2=0.85 for fresh biomass, R^2=0.83 vs R^2=0.73 for dry biomass). Looking at the regression coefficients, camera P tended also to underestimate biomass in comparison with camera C (which could also be seen in Fig 4).

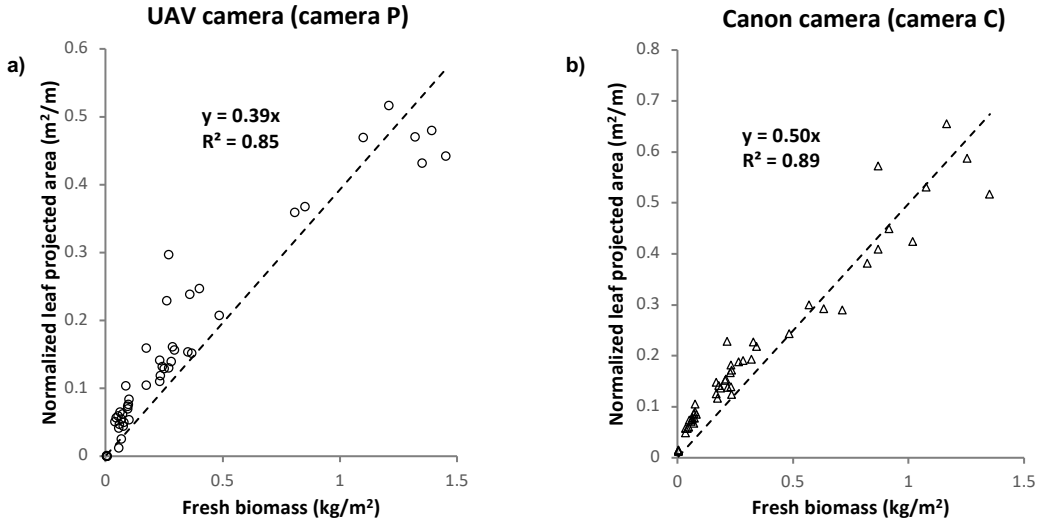

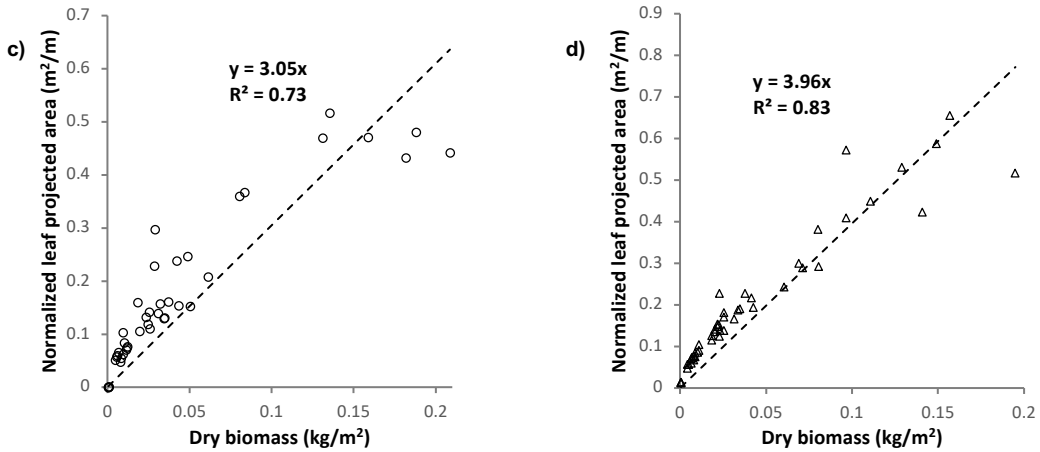

Fig 5. Relationship between fresh (respectively, dry) corn biomass and leaf projected area for cameras P (a, c) and C (b, d), with images taken at zero zenith angle. Sample sizes: N=48 (camera P) and N=50 (camera C).

Comparison between nadir and oblique imagery

Fig 5 (b, d) and Fig 6 compare the effect of viewing angle to assess the leaf projected area, using the measured biomass as ground truth. It can be concluded from those figures that $\widehat{LA}$ could be a good proxy of biomass, regardless of the viewing angles (R^2 varying from 0.89 to 0.95 for fresh biomass, R^2 varying from 0.83 to 0.92 for dry biomass). Although R^2 was slightly lower when the viewing angle is 0°, the regression coefficient was almost constant for the 3 angles.

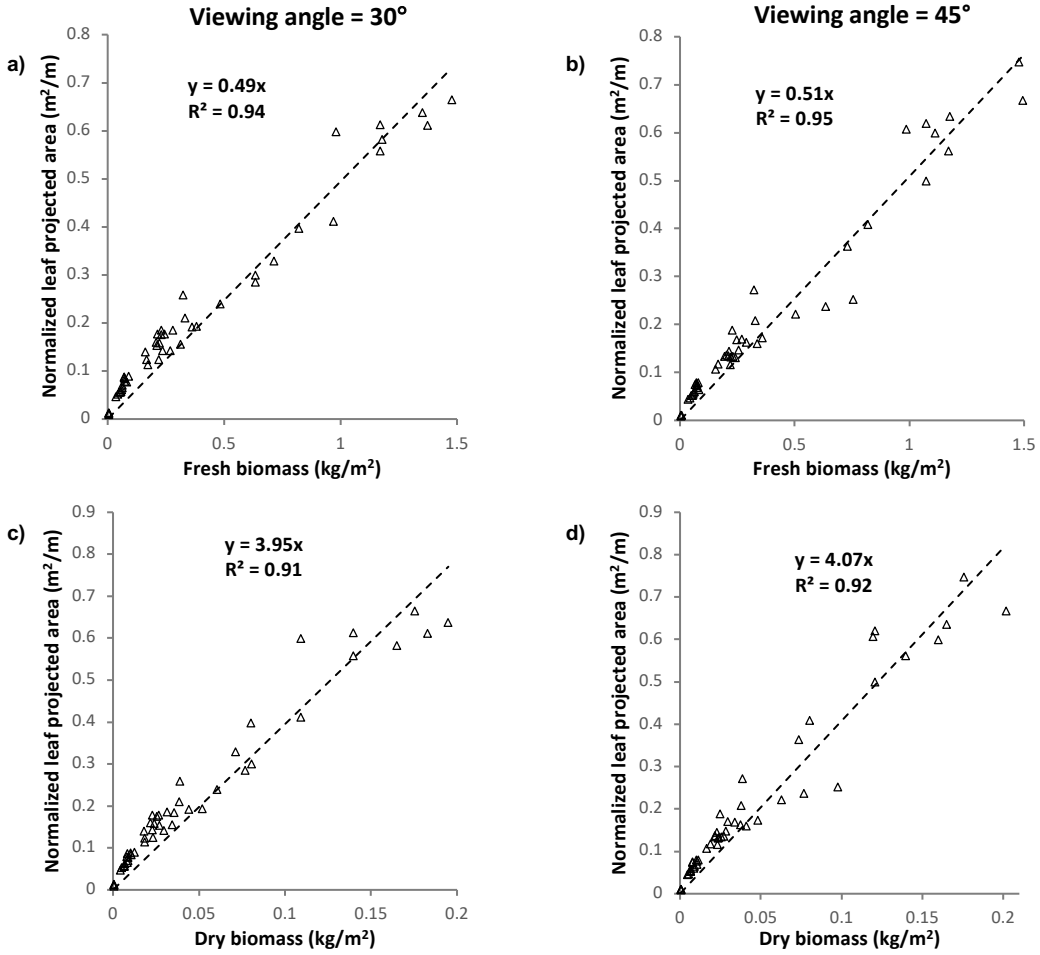

Fig 6. Relationship between fresh (respectively, dry) corn biomass and leaf projected area extracted for camera P, at viewing angles of 30° (a, c) and 45° (b, d). Sample size N=50.

Conclusion

NDVI has been profusely used and is still a popular choice in remote sensing of vegetation. This study explored another way of extracting biomass from images with very high spatial resolution. By segmenting the images and calculating the leaf projected area, it was possible to assess corn biomass with acceptable accuracy. The $\widehat{LA}$ values were slightly more correlated with fresh biomass than dry biomass; when using a fixed camera instead of a moving UAV camera; and with oblique imagery in place of nadir imagery. Despite the necessity of mosaicking and despite the platform instability, UAV performed quite well as long as the spatial resolution was fine enough.

In this study, the ExG – ExR color index was used for the image segmentation, which gave a binary image distinguishing plants from the background. Thus the green pixels did also include weed that was sparsely present in the field despite weeding. A further experiment would require the identification of both types of green pixels: corn and weed. A deep learning algorithm might be a good way of discriminating those vegetation classes, and it could further estimate crop biomass automatically.

Acknowledgements

The authors would like to acknowledge the fine contributions of Morgane Laperle, Arianne Deshaies, Michel Brouillard, Louis Longchamps and Gilles St-Laurent.

References

Berni, J. A. J., Zarco-Tejada, P. J., Suárez, L., & Fereres, E. (2009). Thermal and narrowband multispectral remote sensing for vegetation monitoring from an unmanned aerial vehicle. *IEEE Transactions on Geoscience and Remote Sensing*, 47(3), 722–738.

Bouroubi, Y., Tremblay, N., Vigneault, P., Belec, C., & Adamchuk, V. (2013). Estimating Nitrogen Sufficiency Index using a Natural Local Reference approach. In Proceedings of the Second International Conference on Agro-Geoinformatics (pp. 71–75), doi:10.1109/Argo-Geoinformatics.2013.6621882

Hunt, E. R., Daughtry, C. S. T., Mirsky, S. B., & Hively, W. D. (2013). Remote sensing with unmanned aircraft systems for precision agriculture applications. In Proceedings of the Second International Conference on Agro-Geoinformatics (pp. 131–134), doi:10.1109/Argo-Geoinformatics.2013.6621894

Lelong, C. C. D., Burger, P., Jubelin, G., Roux, B., Labbé, S., & Baret, F. (2008). Assessment of unmanned aerial vehicles imagery for quantitative monitoring of wheat crop in small plots. *Sensors*, 8(5), 3557–3585.

Meyer, G.E., Hindman, T.W., & Lakshmi, K. (1999). Machine vision detection parameters for plant species identification. In G. E. Meyer & J. A. DeShazer (Eds.), Precision Agriculture and Biological Quality 1998, Proceedings of Society of Photo-Optical Instrumentation Engineers (pp. 327–335). Bellingham, WA: SPIE.

Meyer, G. E., & Neto, J. C. (2008). Verification of color vegetation indices for automated crop imaging applications. *Computers and Electronics in Agriculture*, 63(2), 282–293.

Rabatel, G., & Labbé, S. (2016). Registration of visible and near infrared unmanned aerial vehicle images based on Fourier-Mellin transform. *Precision Agriculture*, 17(5), 564–587.

Rasmussen, J., Nielsen, J., Garcia-Ruiz, F., Christensen S., & Streibig, J.C. (2013). Potential uses of small unmanned aircraft systems (UAS) in weed research. *Weed Research*, 53, 242–248.

Woebbecke, D.M., Meyer, G.E., Von Bargen, K., & Mortensen, D.A. (1995). Color indices for weed identification under various soil, residue and lighting conditions. *Transactions of the American Society of Agricultural Engineers,* 38(1), 259–269.

Xue, J., & Su, B. (2017). Significant Remote Sensing Vegetation Indices: A Review of Developments and Applications. *Journal of Sensors*, doi:10.1155/2017/1353691

Yu, Z., Cao, Z., Wu, X., Bai, X., Qin, Y., Zhuo, W., et al. (2013). Automatic image-based detection technology for two critical growth stages of maize: Emergence and three-leaf stage. *Agricultural and Forest Meteorology*, doi:10.1016/j.agrformet.2013.02.011